JOURNAL OF GEOPHYSICAL RESEARCH, VOL. 113, D14201, doi:10.1029/2007JD009150, 2008

Uniform particle-droplet partitioning of 18 organic and elemental components measured in and below DYCOMS-II stratocumulus clouds

L. N. Hawkins,[1] L. M. Russell,[1] C. H. Twohy,[2] and J. R. Anderson[3]

Received 10 July 2007; revised 1 February 2008; accepted 3 March 2008; published 16 July 2008.

[1] Microphysical and chemical aerosol measurements collected during DYCOMS-II research flights in marine stratocumulus clouds near San Diego in 2001 were used to evaluate the partitioning of 18 organic and elemental components between droplet residuals and unactivated particles. Bulk submicron particle (between 0.2 and 1.3 μm dry diameter) and droplet residual (above 9 μm ambient diameter) filter samples analyzed by Fourier Transform Infrared (FTIR) spectroscopy and X-ray Fluorescence (XRF) were dominated by sea salt, ammonium, sulfate, and organic compounds. For the four nighttime and two daytime flights studied, the mass concentration of unactivated particles and droplet residuals were correlated ($R^2 > 0.8$) with consistent linear relationships for mass scavenging of all 18 components on each flight, meaning that the measured particle population partitions between droplet residuals and unactivated particles as if the particles contain internal mixtures of the measured components. Scanning electron microscopy (SEM) for flights 3, 5, and 7 support some degree of internal mixing since more than 90% of measured submicron particles larger than 0.26 μm included sea salt-derived components. The observed range of 0.26 to 0.40 of mass scavenging coefficients for the four nighttime flights results from the small variations in temperature profile, updraft velocity, and mixed layer depth among the flights. The uniformity of scavenging coefficients for multiple chemical components is consistent with the aged or processed internal mixtures of sea salt, sulfate, and organic compounds expected at long distances downwind from major particle sources.

Citation: Hawkins, L. N., L. M. Russell, C. H. Twohy, and J. R. Anderson (2008), Uniform particle-droplet partitioning of 18 organic and elemental components measured in and below DYCOMS-II stratocumulus clouds, *J. Geophys. Res.*, *113*, D14201, doi:10.1029/2007JD009150.

1. Introduction

[2] Aerosol particles affect the Earth's radiation budget directly by scattering light and indirectly by changing cloud properties [*Charlson et al.*, 1992]. Increasing the number of aerosol particles that act as cloud condensation nuclei (CCN) increases the number concentration and decreases the size of droplets in a cloud [*Twomey*, 1977]. The ability of an aerosol particle to act as a CCN is determined by its composition [e.g., *Twohy et al.*, 2001] and size [e.g., *Hegg et al.*, 1993; *Levin et al.*, 2003; *Dusek et al.*, 2006], although composition and size are not independent and both change with location and season. Organic compounds also contribute to the CCN behavior of particles by adding components of limited solubility and reduced surface tension [*Corrigan and Novakov*, 1999; *Facchini et al.*, 1999; *Ming and Russell*, 2004; *Kondo et al.*, 2007; *Ervens et al.*, 2007]. Overall the population of aerosol particles may consist of external mixtures of multiple types of pure components, where the components may include sulfate, nitrate, black carbon, dust, semi and low-volatility organics, fly ash, and sea salt. Individual particles that include multiple components are known as internal mixtures of those components. For internally mixed particles to imply the same CCN-forming properties in the atmosphere, the internal mixture in each particle must contain the same ratio of soluble to insoluble material [*Hansson et al.*, 1998].

[3] Direct measurements of aerosol particles in a range of locations have shown particle populations with external mixtures of qualitatively different compositions [e.g., *Pósfai et al.*, 1995; *Anderson et al.*, 1996; *Väkevä et al.*, 2002; *Li et al.*, 2003; *Brock et al.*, 2004; *Cziczo et al.*, 2004; *Twohy et al.*, 2005b]. Many of these studies show clean marine particles externally mixed with combustion products or mineral components when particles from two or more air masses and different source regions are present. Particles that have

[1] Scripps Institution of Oceanography, University of California San Diego, La Jolla, California, USA.
[2] College of Oceanography and Atmospheric Sciences Oceanography, Oregon State University, Corvallis, Oregon, USA.
[3] Environmental Fluid Dynamics Program, Department of Mechanical and Aerospace Engineering, Arizona State University, Tempe, Arizona, USA.

0148-0227/08/2007JD009150$09.00

several similar components mixed together have been frequently observed in marine-influenced environments [e.g., *Middlebrook et al.*, 1998; *Murphy et al.*, 1998; *O'Dowd et al.*, 1999; *Lee et al.*, 2002; *Sugimoto et al.*, 2002; *Allan et al.*, 2004]. Internally mixed sea salt and organic particles were observed in three of these studies [*Middlebrook et al.*, 1998; *Murphy et al.*, 1998; *Lee et al.*, 2002]. At Trinidad Head, California, *Allan et al.* [2004] observed qualitatively similar mixtures of sulfate and organics in some particles that were separate from other particles containing sea salt components.

[4] The components of particles observed by single particle microscopy and mass spectrometry techniques include a range of ratios of components with each particle type [*Murphy and Thomson*, 1997; *Gao and Anderson*, 2001; *Allan et al.*, 2004]. For example, particles with varying fractions of sulfate, and hence varying CCN activity, will be grouped together in a single type by some single particle techniques. Since different ratios of components will have different properties, particles classified by qualitative single particle techniques as internally mixed may have different properties even though they contain the same components. By measuring the solubility, water uptake, surface tension, and scavenging of ambient aerosol, particles can be classified by their properties rather than (or in addition to) their composition. For assessing aerosol-cloud interactions, these two approaches have been used to measure differences in particle properties and behavior. The first uses solubility, hygroscopicity, or surface tension of particles to predict the activation of particles to droplets. The second approach uses mass scavenging coefficients to quantify the partitioning of droplets and particles, by both activation of CCN and scavenging of interstitial particles within the cloud. The second approach can be extended to provide additional information on both composition and mixing by measuring mass scavenging for multiple chemical components simultaneously.

[5] The mass scavenging coefficient (F) quantifies the tendency of a particular chemical component to be incorporated into cloud droplets [*Baltensperger et al.*, 1998] and has been used to differentiate particle types that partition into cloud droplets and interstitial particles with different efficiencies [*Hallberg et al.*, 1992; *Mertes et al.*, 2001; *Sellegri et al.*, 2003]. While the measured differences in mass scavenged fraction are useful to describe some aspects of particle composition, there is insufficient information in this measurement to quantify the composition of each particle. For any chemical component,

$$F = \frac{M_{\text{residual}}}{M_{\text{total}}} \tag{1}$$

where M_{residual} is the droplet residual mass and M_{total} is the total mass of the component in both the particle and droplet phases. For external mixtures, each component could have a unique mass scavenging coefficient depending on its hygroscopicity. *Baltensperger et al.* [1998] found sulfate near $F = 1$ for submicron particles at a high-alpine site in the Bernese Alps. A similar study at a remote marine site found the sulfate activation fraction to be closer to 0.8, where sulfate concentrations were between 0.2 and 2 μg m^{-3} [*Heintzenberg and Leck*, 1994]. For an internal mixture with the same fraction of each component, mass scavenging coefficients will be constant for all components even if the components have different hygroscopic properties.

[6] *Hallberg et al.* [1992] found sulfate externally mixed with elemental carbon on the basis of the observed scavenged fraction (0.18 and 0.06, respectively). Similarly, *Sellegri et al.* [2003] identified particles as internal mixtures of elemental carbon and sulfate, ammonium, or nitrate based on the higher mass scavenging coefficient obtained for elemental carbon (F = 0.33) than organic carbon (F = 0.14). In addition, they determined the organic aerosols to be externally mixed from those inorganic species (F = 0.76). *Mertes et al.* [2001] report similar mass scavenging values for organic carbon, sulfate, sodium, and ammonium (from 0.49 to 0.55) and smaller scavenging coefficients for both black carbon (0.17) and graphitic carbon (0.14), indicating that black carbon and graphitic carbon were in separate particles from those that contained a mixture of organic carbon, sulfate, sodium, and ammonium. *Heintzenberg and Leck* [1994] show that sulfate and elemental carbon have similar scavenging efficiencies for polluted and remote marine regions, but they have very different scavenging efficiencies over continental regions, illustrating that different particle-droplet partitioning may be caused by source-based differences such as varying the fractions of sulfate and elemental carbon or including other components.

[7] Here we present the measured chemical composition of particles and droplet residuals during the Dynamics and Chemistry of Marine Stratocumulus-II (DYCOMS-II) experiment from 2001. The meteorological characteristics of the stratocumulus layers (including entrainment and drizzle) observed for the seven nighttime and two daytime research flights are described by *Stevens et al.* [2003]. *Twohy et al.* [2005a] showed that DYCOMS-II below-cloud particle number concentrations (0.1 to 3.0 μm diameter) were correlated positively with droplet number concentrations and negatively with droplet size. This work reports the mass scavenging coefficients for a series of chemical components measured in and below cloud. These component-specific mass scavenging coefficients are used to evaluate if the partitioning of those components between unactivated particles and droplet residuals is consistent with that expected for particles with the same internal mixtures of components at fixed ratios. Both below-cloud and interstitial unactivated particles were measured to compare their partitioning behavior and the spatial homogeneity of the sampled air masses.

2. Method

[8] Aerosol and cloud properties were measured during the DYCOMS-II experiment off the coast of San Diego in July 2001. The aim was to characterize the chemistry and microphysics of marine stratocumulus clouds lying within a well-mixed boundary layer. Most flights in the NCAR C-130 aircraft consisted of a ferry leg to approximately 300 km offshore, followed by a series of circles in, above, and below cloud. The research flights each attempted to follow the advection of a single air mass, however, wind shear and flight pattern restrictions prevented the flight paths from being strictly Lagrangian [*Stevens et al.*, 2003]. Six flights

Table 1. Particle Measurements Aboard the NCAR C-130 During DYCOMS-II

Instrument	Sample Type	Quantity Measured	Size Range, μm
	Inlets		
Counterflow virtual impactor (CVI)	droplet	droplet residual chemical composition	9 to 50
Solid diffuser inlet (SDI)	particle	particle chemical composition	0.2 to 1.3
Low turbulence inlet (LTI)	particle	single particle SEM and TEM	<6[a]
	Spectrometers		
Forward scattering spectrometer probe (FSSP-100)	droplet	droplet size distributions	2 to 47
Passive cavity aerosol spectrometer probe (PCASP-100)	particle	particle size distributions	0.1 to 3

[a]Estimated from losses by impaction on plumbing walls [*Huebert et al.*, 2004, Figure 6].

are analyzed here: flights 3, 4, 5, and 7 measured between 2200 and 0600 local time, and flights 8 and 9 measured between 1100 and 2200 local time. Samples from flights 3, 4, and 5 were collected during circles which were constant within 20 m, and samples from flights 7 and 8 were constant within 50 m. Flight 9 did not contain constant altitude circles, so samples spanned 200 to 400 m vertically, reducing the accuracy of the reported concentrations. Flights 1 and 2 did not collect cloud droplet residuals and are omitted from this analysis. Stratocumulus decks were dense and generally uniform, and drizzle was common with an average 0.5 mm d^{-1}. More detailed information on flight patterns and meteorological conditions is provided by *Stevens et al.* [2003].

[9] Five aerosol instruments and inlets on the C-130 aircraft were used to measure particle and droplet size and to collect samples for the size ranges in Table 1. Particle size distributions were recorded by the wing-mounted Particle Measuring Systems Passive Cavity Aerosol Spectrometer Probe (PCASP-100x). The PCASP measures number concentrations across nominal size bins ranging from 0.1 to 3.0 μm with 1 s resolution, where the size measured is assumed to be dry [*Strapp et al.*, 1992]. Spikes and negative values were removed prior to analysis. Cloud droplet (2 to 47 μm) size distributions were measured during flights 3, 4, 7, 8, and 9 with the Forward Scattering Spectrometer Probe (FSSP-100) [http://www.eol.ucar.edu/raf/Bulletins/B24/fssp100.html]. The FSSP optical particle counter uses Mie theory to calculate the size of each particle based on the intensity of the scattered light. Flight 5 droplet concentrations were calculated from the "fast-FSSP" [*Brenguier et al.*, 1998] because the FSSP-100 instrument data were not available [*vanZanten et al.*, 2005]. The two instruments provide comparable measurements for the drop size and number concentration ranges measured here [*Burnet and Brenguier*, 2002].

[10] Cloud droplet residual composition was determined using a counterflow virtual impactor (CVI) inlet, which isolates cloud droplets larger than approximately 9 μm at aircraft speeds of 100 m s^{-1} in a stream of nitrogen gas flowing out through the CVI tip [*Twohy et al.*, 2001]. The droplets are dried and the nonvolatile residual mass is collected on 37 mm stretched Teflon filters (Teflo Membrane, Pall Corp., Ann Arbor, MI). A small impactor (0.55 μm cut dried diameter) was installed upstream of the filters to provide an equivalent upper size cut to the impactor used in the solid diffuser inlet (SDI) sampling system (1.3 μm cut ambient diameter). The 0.55 μm cut size was used to correct for the expected difference in relative humidity between the ambient humidity SDI and dried CVI samples (assuming growth factors for NaCl). The filters were analyzed by Fourier Transform Infrared (FTIR) spectroscopy [*Maria et al.*, 2003] and X-ray Fluorescence (XRF) to provide mass concentrations for (organic and inorganic) functional groups and elements, respectively. XRF analysis was performed by Chester Labs [*Maria and Russell*, 2005]. All concentrations that were less than or equal to the detection limit were removed. Elevated levels of chloride and sulfur in the CVI at lower relative humidity were associated with bouncing of dried supermicron sea salt particles, which artificially enhanced the mass collected on the Teflon filters. This artifact was measured in the laboratory as a function of dry size by comparison of NaCl to ammonium sulfate particles, and the resulting calibration curve was used to correct the chloride and sea salt sulfur, sulfate, potassium, and calcium concentrations. The correction factor R was applied as in equation (2),

$$Cl_{\mathrm{m,submicron}} = Cl_{\mathrm{m,tot}} - \frac{Cl_{\mathrm{c,tot}} - Cl_{\mathrm{c,submicron}}}{R} \qquad (2)$$

where m and c denote measured and calculated values, respectively. Chloride is used as a marker for unreacted sea salt (NaCl), which may underestimate total sea salt concentrations due to loss of some chloride mass as HCl gas [*Seinfeld and Pandis*, 1998]. SEM measurements indicate that a majority of supermicron particles were sea salt for flights 3, 5, and 7. Bouncing of the reacted supermicron sea salt particles (which account for between 19% and 55% of supermicron particles) is less likely than unreacted sea salt particles (which account for between 34% and 87% of supermicron particles) [*Boskovic et al.*, 2005; *Brach et al.*, 2000; *Li et al.*, 2003], making chloride an appropriate surrogate for the unreacted sea salt particles which represent the bounced fraction of supermicron particles.

[11] Sea salt stoichiometric ratios [*Warneck*, 1988] were used to determine and correct the sea salt contributions of sulfur, sulfate, potassium and calcium concentrations. The uncertainty associated with this correction scales with the fraction of the component that is from sea salt, which is a large fraction of the chloride and a smaller fraction of the sulfur, sulfate, potassium, and calcium. Correction factors for chloride are on the order of 0.04 while those for sulfur, sulfate, potassium, and calcium are between 0.5 and 0.7.

[12] DYCOMS-II particles between 0.2 and 1.3 μm were collected using the solid diffuser inlet (SDI) [*Huebert et al.*, 2004]. The SDI was followed by a three-stage particle concentrator (3SPC) consisting of three slit virtual impac-

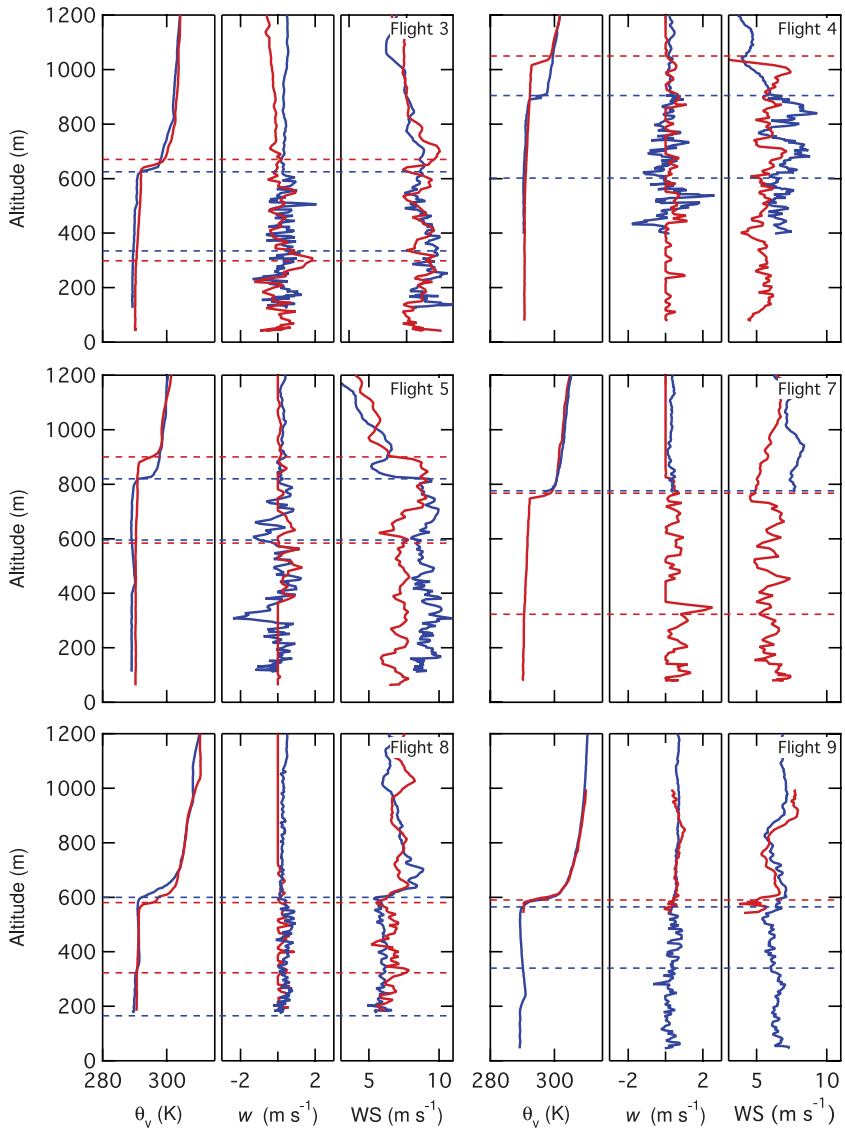

Figure 1. Altitude profiles of virtual potential temperature (θ_v), vertical velocity (w) and horizontal wind speed (WS) for the six research flights. Multiple lines indicate multiple measured profiles within each flight and are differentiated by line color with blue lines at the beginning of the flight and red lines at the end. Horizontal dashed lines mark cloud top and bottom, and are derived from LWC. Virtual potential temperature is used to mark cloud top for profiles in flights 4, 7, and 9 where LWC is not available.

tors, which concentrated the volume of particles collected on the Teflon filters by up to a factor of 19 [*Maria et al.*, 2002]. These Teflon filters were analyzed by FTIR spectroscopy and XRF. Both particles and cloud droplets were sampled to provide below and in-cloud concentrations (μg m^{-3} of air sampled) for each chemical component.

[13] A porous diffuser low turbulence inlet (LTI) following the design of *Huebert et al.* [2004] was used to collect single particles less than 6 μm on polycarbonate membrane filters with a Streaker (PIXE International) for SEM (>0.26 μm). Smaller particles (<0.26 μm) were collected by a 3-stage impactor following the LTI for transmission electron microscopy (TEM). The four different types of samples collected were designated as "below-cloud particles" (sampled through the SDI, discussed in section 3.2.1), "in-cloud or interstitial particles" (sampled through the SDI, discussed in section 3.2.2), "droplet residuals" (sampled through the CVI, discussed in section 3.3), and "single particles" (sampled through the LTI and analyzed by SEM and TEM, discussed in section 4.2).

3. Results

[14] During each flight aerosols and clouds were characterized by particle size distribution, vertical concentration profile, and mass scavenging efficiency. Flights 4, 7, and 8 were clean relative to marine conditions, with less than 250 cm^{-3} (where we have identified flights as clean based on low below-cloud condensation nuclei (CN) number concentration) while flight 9 was closer to shore and

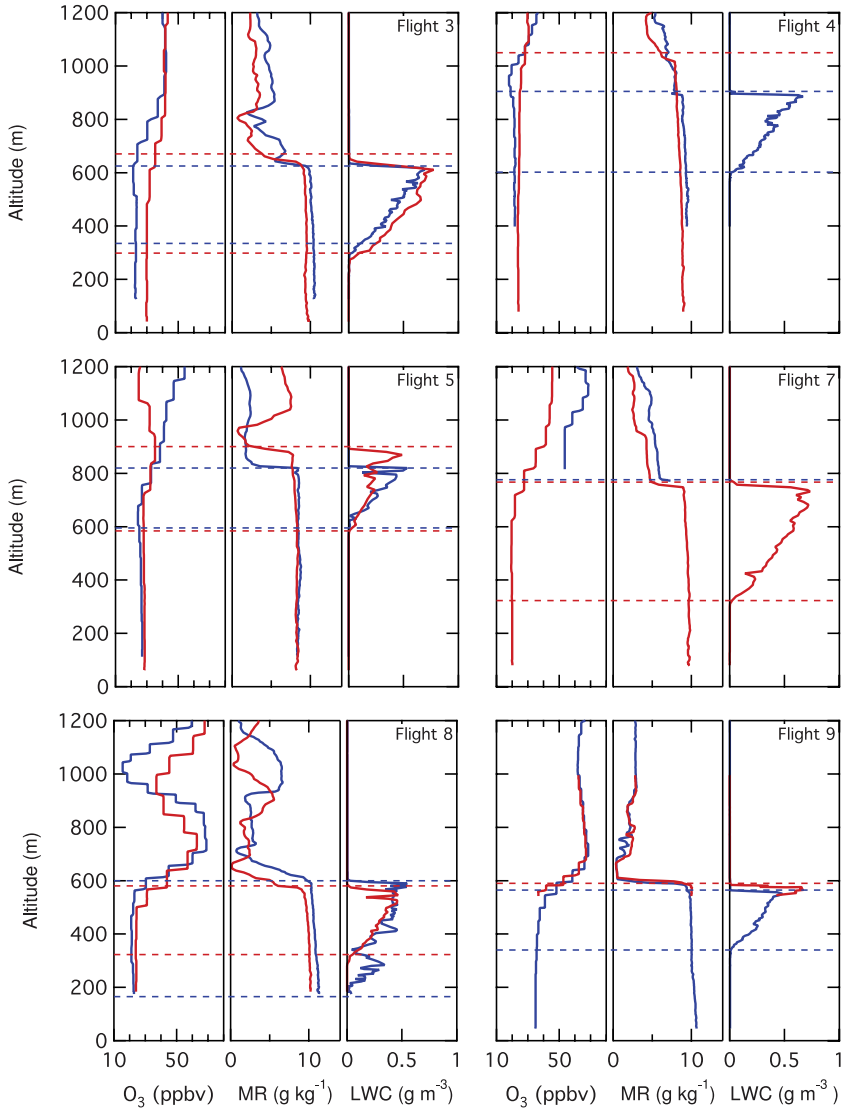

Figure 2. Altitude profiles of ozone (O_3), water mixing ratio (MR), and liquid water content (LWC) for flights 3, 4, 5, 7, 8, and 9. Line colors are the same as Figure 1.

relatively polluted, with greater than 400 cm^{-3}. The concentrations during flights 3 and 5 are between 250 and 300 cm^{-3}.

3.1. Meteorological Conditions

[15] Figures 1 and 2 show vertical profiles of virtual potential temperature (θ_v), vertical velocity (w), horizontal wind speed (WS), ozone mixing ratio, water mixing ratio (MR), and liquid water content (LWC) for each research flight. Profiles were measured near the beginning and end of each 9 h flight. Comparing the profiles for each flight shows few changes in temperature, updraft, water vapor, and ozone mixing ratio profiles between the start and end of sampling. The depth of the mixed layer obtained from virtual potential temperature, liquid water content, or water mixing ratio varies between 560 m and 1020 m and marks the cloud top altitude (Table 2): flights 8 and 9 have shallow mixed layers (less than 600 m). Vertical velocity and wind speed profiles are consistent with other markers of mixed layer depth and show reduced updrafts in and shear at the boundary between the mixed layer and the free troposphere. The average liquid water content in cloud ranges from 0.19 to 0.43 g m^{-3} and was the highest in flight 7, which had the thickest cloud layer observed during vertical profile measurements. The standard deviations of vertical velocity during these sample periods range from 0.39 to 0.74 m s^{-1} (Table 2).

3.2. SDI Particle (0.2 to 1.3 μm) Size and Composition

[16] Figures 3a and 3b show below-cloud and interstitial particle composition, respectively. Compounds are divided into categories based on their reactive properties and origin. Metals and mineral components include aluminum, titanium, chromium, manganese, iron, copper, vanadium, cobalt, nickel, potassium, calcium, silicon, and silicate ions. The ammonium and sulfate category also includes elemental sulfur since the latter is dominated by sulfate [*Seinfeld and Pandis*, 1998]. The organic category reflects the total measured amounts of saturated aliphatic C-C-H, carbonyl C = O, and organosulfur C-O-S; the latter two were above

Table 2. Cloud Structure and Mixing for Stratocumulus Layers in DYCOMS-II

Flight	Cloud top[a,b], m	Cloud Bottom[a,b], m	Cloud Mean LWC[a], g m^{-3}	MR[a,c], g kg^{-1}	WS[a,c], m s^{-1}	Standard Deviation in w[d], m s^{-1}	Avg. Drizzle Rate, mm d^{-1}
3	625	300	0.37	10.5	11.6	0.72, 0.70, 0.58, 0.59, 0.74	0.05 ± 0.03
	650	270	0.42	9.5	11.1		
4	900	605	0.32	9.4	6.9	0.69, 0.69, 0.62, 0.64	0.08 ± 0.06
	1020[e]	n/v	n/v	n/v	5.6		
5	820	630	0.25	8.5	9.1	0.43, 0.61, 0.66	BDL
	880	595	0.19	8.3	7.5		
7	770[e]	n/v	n/v	n/v	n/v	0.67, 0.69, 0.60, 0.60	0.60 ± 0.18
	770	340	0.43	9.6	6.1		
8	595	205	0.29	11.2	5.9	0.39, 0.42, 0.49	0.12 ± 0.03
	580	300	0.26	10.2	6.5		
9	560	350	0.25	10.3	6.3	n/v	n/v
	585	n/v	n/v	n/v	n/v		

[a]Vertical profile mean values (Figures 1 and 2). Most flights have two vertical profiles.
[b]Cloud top and bottom altitudes as measured by cloud liquid water content (LWC).
[c]Mean value of wind speed (WS), bounded by the temperature inversion. Mean value of mixing ratio (MR) is below cloud level only.
[d]Multiple vertical velocities for each flight represent individual flight circles along a constant altitude (Figure 3).
[e]Cloud top levels were based on virtual potential temperature since LWC was unavailable. Cloud bottom altitude was not available for these profiles.

detection limit in less than 5% and 12% of the samples, respectively, and provide insufficient data for comparison of droplet and particle composition. Chloride is measured by XRF and reflects the unreacted sea salt fraction [*Seinfeld and Pandis*, 1998].

[17] Panels in Figure 4 show the interstitial and below-cloud particle size distributions measured by the PCASP, averaged for the SDI sampling periods. The PCASP measured continuously for the duration of the flight (approximately 9 h); the SDI was only used to collect particles during constant altitude circles lasting 30 min to 1 h. The below-cloud distributions are characterized by a broad peak near 0.2 μm of varying concentration (Table 3). Mass-mean ($\overline{D}_{m,SDI}$) and number-mean ($\overline{D}_{SDI}$) diameters of particles within the SDI cutoff size range of 0.2 to 1.3 μm for the six flights range from 0.89 to 1.1 μm and from 0.28 to 0.36 μm, respectively (Table 4). Size distributions in all flights show higher concentrations of smaller particles (<0.5 μm) in below-cloud than in interstitial samples. Flights 3, 4, 5, 7, and 8 show smaller below-cloud $\overline{D}_{m,SDI}$ (0.48 to 0.66 μm) than interstitial $\overline{D}_{m,SDI}$ (0.84 to 1.12 μm) (Figure 4).

[18] Vertical profiles of concentrations of the chemical components collected by the SDI during each flight are illustrated in Figure 5. The two interstitial samples for flight 9 were collected at altitudes that varied by ±200 m including cloud top and bottom within each circle. Within each flight the relative proportions of most chemical components are consistent at the sampling altitudes, indicative of well-

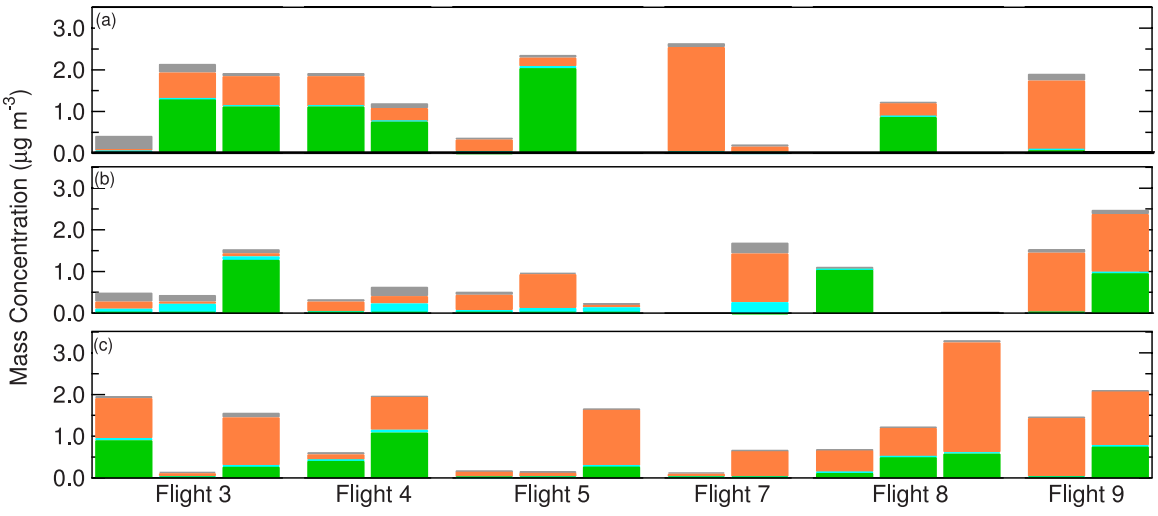

Figure 3. Mass concentration of (a) SDI particles below-cloud, (b) SDI particles in-cloud, and (c) CVI droplet residual particles. Metals and mineral components (grey) include aluminum, titanium, chromium, manganese, iron, copper, vanadium, cobalt, nickel, potassium, calcium, silicon, and silicate ions. The ammonium and sulfate category (orange) also includes elemental sulfur. Organic compounds (green) include saturated aliphatic C-C-H, carbonyl C = O, and organosulfur C-O-S although only 5% of samples had carbonyl above detection limit and 12% of samples had organosulfur above detection limit. Chloride is grouped alone (turquoise). Individual bars represent 30 min or 1 h continuous sampling periods. The number of samples taken varies by flight and by sample type.

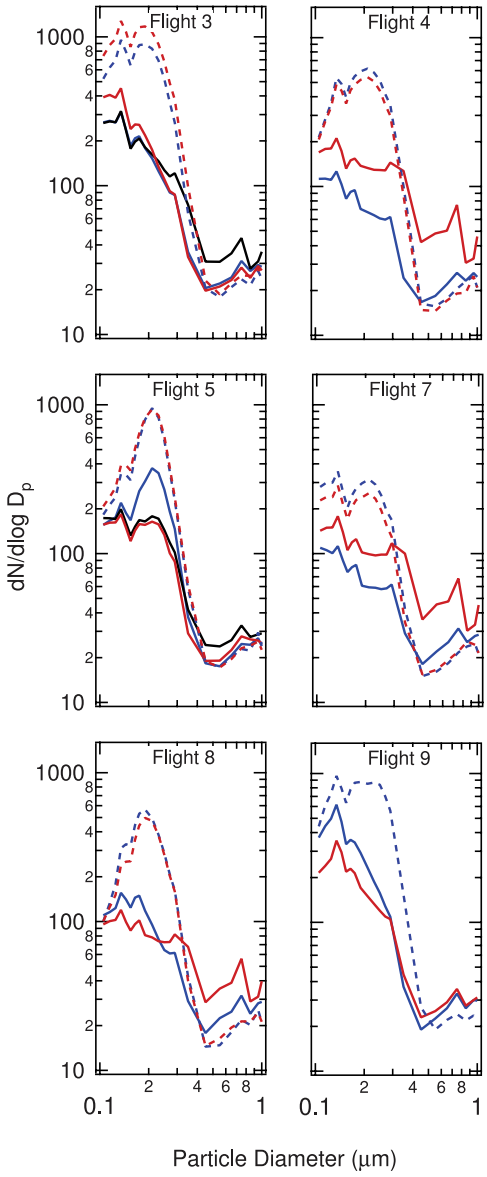

Figure 4. Panels contain the PCASP particle size distributions for the SDI size range and sampling intervals (between 30 min and 1 h) during each flight. dN/dlogD_p values are plotted against particle diameter. Solid lines represent interstitial particle measurements averaged over a constant altitude sampling circle. Dashed lines represent below-cloud measurements averaged over a constant altitude sampling circle. Blue, black, and red lines mark samples collected at the beginning, middle, and end of the flights, respectively.

mixed air masses, although there are some minor differences. All components show similar concentration profiles for the 6 flights.

3.2.1. Below-Cloud Particles

[19] All below-cloud sample particle number distributions have a mode centered between 0.18 and 0.25 μm, which we will refer to as the 0.2 μm mode (Figure 4), with a shoulder or second mode at a smaller diameter. The 0.2 μm number mode corresponds to a mean mass diameter of about 0.55 μm. Below-cloud distributions have a very small number of particles in a mode centered between 0.76 and 0.83 μm. In the 0.13 to 0.14 μm size bin, flight 9 had 47 cm^{-3}, the highest dN/dlogD_p peak concentration for the project. The below-cloud particle peak number concentrations are uniform within each of the six research flights, with little variation in mode diameter between samples or flights (Table 3).

[20] Ammonium and sulfate make up the largest identified portion of the below-cloud particle mass for most flights, with an average mass concentration of 1.5 μg m^{-3} and mass fractions that range from less than 1% to 95% (Figure 3a). Below-cloud organic mass concentrations range from below the detection limit to 2.0 μg m^{-3} and the organic mass fraction ranges from less than 1% to 87%. Below-cloud chloride was present in the largest concentration in flight 3 at 0.07 μg m^{-3}.

3.2.2. Interstitial Particles

[21] The interstitial number distributions in Figure 4 show a smaller peak in the 0.2 μm mode (corresponding to a mass-mean diameter of about 1.1 μm) than is present in the below-cloud distributions, with between 63% and 73% of the particles having been removed or grown to droplets (Table 3). Flight 9 has the highest concentration of interstitial submicron particles, as well as a broad peak at 0.2 μm. The 0.8 μm interstitial mode has between 2 and 4 times higher concentrations than below-cloud, with significant variability both between and within the flights. Flights 4, 7, and 8 are relatively clean and have larger variations in interstitial particle size distributions between the sampling intervals than flights 3, 5, and 9, which have higher CN concentrations on average (Figure 4). Flights 4, 7, and 8 also have higher drizzle rates (0.08 to 0.60 mm d^{-1}) than flights 3, 5, and 9 (below detection limit to 0.05 mm d^{-1}) (Table 2) and have heavy drizzle events contributing to between 20% and 64% of the total drizzle (Table 1) [*vanZanten et al.*, 2005]. The differences in the in-cloud interstitial particle distributions, despite very similar ozone mixing ratios during flights 4, 7, and 8, probably result from these heavy drizzle events.

[22] Ammonium and sulfate dominate the interstitial particle mass, with an average mass concentration of 1.0 μg m^{-3} (Figure 3b). The interstitial organic mass concentration varied the most between flights, ranging from below detection limit to 1.28 μg m^{-3}. Elevated chloride

Table 3. PCASP Particle Size Distribution Properties for 0.2 μm Particle Mode

Flight	BC Peak Diameter[a], μm	BC Concentration[a], dN/dlogD_p in cm^{-3}	Decrease in 0.2 μm Mode In-Cloud[b], %
3	0.19	890	73
	0.19	1200	
4	0.21	620	72
	0.21	540	
5	0.21	950	63
	0.21	930	
7	0.21	320	58
	0.21	250	
8	0.19	570	66
	0.19	500	
9	0.23	880	65

[a]Diameters and concentrations are given for each below-cloud (BC) sample within a given flight.

[b]The difference between the average number concentrations of below-cloud and interstitial particles smaller than 0.35 μm.

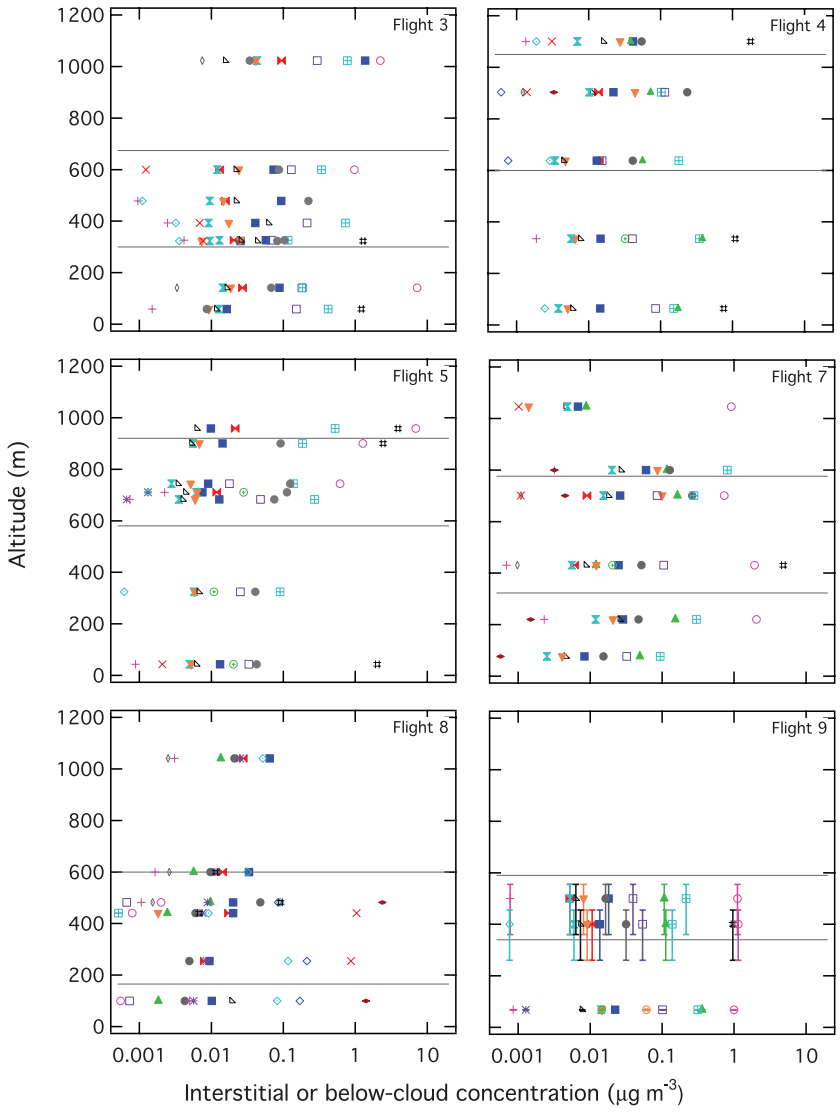

Figure 5. Panels contain the vertical distribution of species collected by the SDI in, above, and below the cloud level. Grey lines mark the greatest vertical extent of cloud layer from Figures 1 and 2. Markers show: aluminum (solid red bowtie), silicon (solid blue square), sulfur (solid green upward triangle), potassium (solid turquoise vertical bowtie), calcium (solid orange downward triangle), vanadium (purple asterisk), iron (open black triangle), ammonium (open turquoise quartered square), sulfate (open pink circle), titanium (open grey narrow diamond), manganese (red x-cross), cobalt (open blue diamond), organosulfur C-O-S (open green circle with plus), nickel (solid dark red wide diamond), carbonyl C = O (open orange circle with x-cross), silicate (open purple square), aliphatic C-C-H (black pound), copper (open turquoise diamond), chromium (pink plus), and chlorine (solid grey circle). Vertical error bars indicate the altitude range of the sample when it exceeds ±20 m, which is only for flight 9.

concentrations in interstitial particles relative to below-cloud particles and droplets may be attributed to the increased partitioning of semivolatile chloride into unactivated particles in-cloud relative to below-cloud because of their larger water uptake. Interstitial chloride was highest in flight 7 at 0.26 μg m^{-3}.

3.3. Droplet Mode Size and Droplet Residual Composition

[23] Droplet size and concentration were measured by the FSSP-100 and fast-FSSP probes, with the mean diameter for each flight ranging from 6.6 to 11.3 μm. Figure 6 is similar to Figure 3 from *Twohy et al.* [2005a], where we have modified the data on the abscissa. Droplet number concentration measured by the FSSP and fast-FSSP shows a strong dependence on particle number concentration (0.2 to 1.3 μm only) measured by the PCASP (R^2 = 0.76), in agreement with the correlation of droplet number concentration and particle number concentration of the PCASP size range (0.1 to 3 μm) used by *Twohy et al.* [2005a]. Drop size is also correlated (inversely) with particle number concentration (R^2 = 0.69). The most polluted flight (9) has the highest droplet concentration and the lowest mean droplet diameter [*Twohy et al.*, 2005a]. The two cleanest flights 7

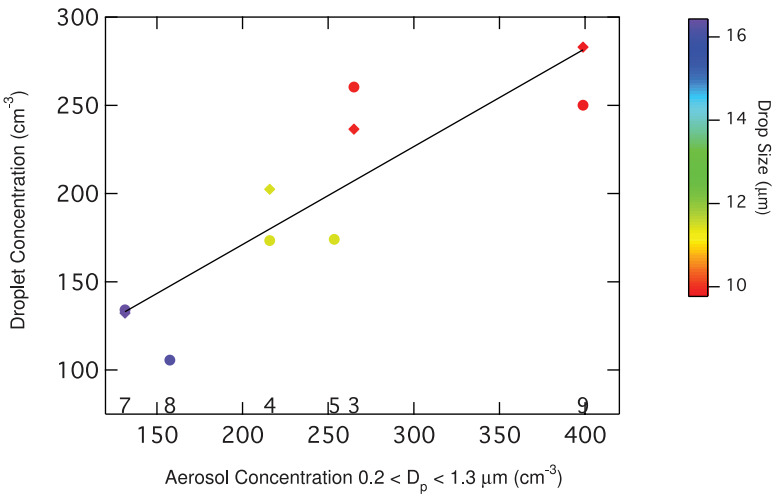

Figure 6. Droplet concentration as a function of particle number concentration for 0.2 to 1.3 um diameter particles. Color indicates droplet size as measured by the FSSP-100 for flights 3, 4, 7, 8, and 9 and fast-FSSP for flight 5. Droplets are defined by the two FSSP probes as cloud particles above 2 μm. Values along the y = 0 line are flight number, and correspond to the markers above them. Shaded diamonds and shaded circles correspond to cloud bottom and cloud top, respectively. The best fit line (y = 0.55x + 60) has an $R^2 = 0.76$. Drop size correlates to particle number concentration ($R^2 = 0.69$).

and 8 have the largest drops and lowest droplet concentrations, respectively.

[24] Chemical composition of droplet residual mass is shown in Figure 3c, with multiple samples acquired during each flight. Ammonium and sulfate constitute the bulk of the mass collected (above 0.5 μg m^{-3} in 10 of 15 samples) and from 22% to 95% of measured residual mass. Organic compounds also contribute significantly to residual mass (below detection limit to 1.1 μg m^{-3}), from less than 1% to 56%. Chloride is observed at lower concentrations in the droplet residuals than in interstitial particles, perhaps resulting from increased loss of chloride as HCl during cloud processing in aqueous cloud droplets (which are less acidic than interstitial particles) or during sampling and evaporation in the CVI.

3.4. Mass Scavenging Coefficients and Cutoff Diameter

[25] Following equation (1), flight-averaged droplet residual concentrations M_{residual} for each component measured are shown to depend on the total concentration of that component M_{total}, which is the sum of the flight-averaged in-cloud particle (interstitial) concentration $M_{\text{interstitial}}$ and the droplet residual concentration M_{residual} (Figure 7). This plot yields the mass scavenging coefficient F_{in} (equation (3)) as the slope of the line.

$$F_{\text{in}} = \frac{M_{\text{residual}}}{M_{\text{residual}} + M_{\text{interstitial}}} \tag{3}$$

For below-cloud samples, M_{total} is $M_{\text{below-cloud}}$ and we can rewrite equation (3) as,

$$F_{\text{below}} = \frac{M_{\text{residual}}}{M_{\text{below-cloud}}} \tag{4}$$

Here the slope of the line generated by plotting cloud droplet residual concentration against below-cloud particle concentration yields F_{below}.

[26] Mass scavenging coefficients for each sampling interval were used with PCASP number distributions to calculate the cutoff diameter D_p^* below which particles form droplets smaller than the lower size cut of the CVI (9 μm). First the total mass (M_{SDI}) of particles in the SDI size range was determined (equation (5)).

$$M_{SDI} = \int_{D_p=0.2\ \mu\text{m}}^{D_p=1.3\ \mu\text{m}} \frac{D_p^3}{6}\pi\rho N_p\ dD_p \tag{5}$$

where ρ is the density of water and N_p is the number of particles in each size bin. From the mass scavenging fraction (F) and the total particle mass (M_{SDI}), D_p^* is defined implicitly as

$$(1-F)M_{SDI} = \int_{D_p=0.2\ \mu\text{m}}^{D_p=D_p^*} \frac{D_p^3}{6}\pi\rho N_p\ dD_p \tag{6}$$

The values for particle number (N_p) are binned such that D_p^* precision is limited by the width of the measured size bins.

4. Discussion

4.1. Uniform Particle-Droplet Partitioning of 18 Chemical Components

[27] For spatially well-mixed, clean, low SO_2 air masses the bulk below-cloud and total (particle plus droplet) in-cloud composition of nonvolatile components will be comparable and will result in similar F_{in} and F_{below} values. For less homogeneous regions, the below-cloud samples and interstitial samples collected in spatially and temporally separated air masses will be more variable. Flights 4 and

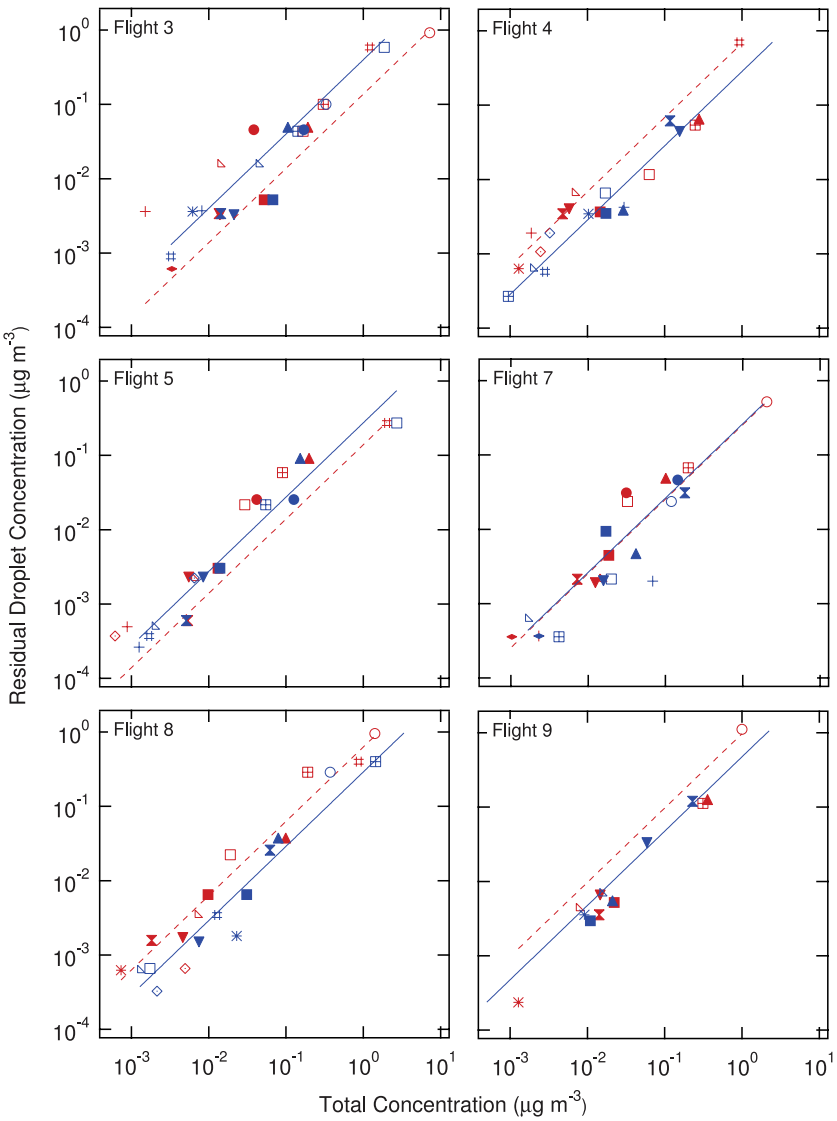

Figure 7. Panels contain the mass scavenging coefficient plots. Concentrations of components in droplet residuals are plotted on the ordinate (CVI); total concentrations in and below-cloud level are plotted on the abscissa. Marker shape is consistent with Figure 5. Blue markers and the blue solid fit line represent flight-averaged concentrations within the cloud, the red markers and the red dashed fit line represent below cloud samples. Scavenging coefficients (F) range from 0.14 to 0.97 below cloud and 0.26 to 0.40 in cloud. Best fit values for each panel are given in Table 6.

7 were chemically homogeneous in space and time, showing little change in mean ozone mixing ratio between sampling circles (1–3 ppbv) and small standard deviations within each circle (0.6–1.5 ppbv, as in Table 5). For flight 7 the mass scavenging coefficients were also consistent between the below and in-cloud measurements (Table 6). Flight 4 had homogeneous ozone mixing ratios and particle compositions, but the mass scavenging coefficients in and below-cloud differed by a factor of 2. This difference may result from the missing (below detection limit) measurements of concentration of saturated aliphatic C-C-H in interstitial particles for both in-cloud circles during flight 4, since the organic mass scavenging coefficient has a significant influence on the line fit for the average mass scavenging coefficient. Chemical variability was higher in the more polluted flights (3 and 5, with 8–16 ppbv differ-

Table 4. Mass and Number Size Distribution Properties for Particles Collected by the SDI (0.2 to 1.3 μm) and PCASP (0.1 to 3 μm)

	SDI Fraction[a]		Mass-Mean Diameter, $\overline{D}_m$, μm		Number-Mean Diameter, $\overline{D}$, μm	
Flight	Mass %	Number %	0.2 to 1.3 (SDI)	0.1 to 3.0 (PCASP)	0.2 to 1.3 (SDI)	0.1 to 3.0 (PCASP)
3	3.3	31	0.96	2.5	0.30	0.24
4	3.1	46	1.0	2.6	0.35	0.35
5	3.9	52	0.92	2.5	0.28	0.23
7	3.1	28	1.1	2.6	0.36	0.31
8	2.8	28	1.0	2.6	0.32	0.26
9	3.5	27	0.89	2.5	0.29	0.20

[a]SDI fraction is the number or mass fraction of particles between 0.2 and 1.3 μm relative to the particles between 0.1 and 3.0 μm.

Table 5. Mean and Standard Deviation of Ozone Mixing Ratios Within and Between Constant Altitude Circles

Flight 3	Flight 4	Flight 5	Flight 7	Flight 8	Flight 9
Mean and Standard Deviation of O_3 in Each Circle, ppbv					
26 ± 3.9	23 ± 0.58	26 ± 1.5	17 ± 1.5	23 ± 1.4	35 ± 0.89
27 ± 4.2	23 ± 0.37	34 ± 8.9	18 ± 1.1	23 ± 1.5	35 ± 0.60
26 ± 4.1	24 ± 0.35	27 ± 1.1	19 ± 1.1	23 ± 1.3	34 ± 0.39
26 ± 3.9	24 ± 0.50	28 ± 1.1	19 ± 1.1	23 ± 1.4	
42 ± 2.4	24 ± 0.39	28 ± 1.3	20 ± 0.94	23 ± 2.1	
32 ± 1.9	24 ± 0.37		19 ± 1.0		
32 ± 1.8					
Standard Deviation Among Circles					
6.0	0.62	3.2	0.95	0.089	0.68

ences in mean ozone mixing ratios between sampling circles) and the day flights 8 and 9. The poor correlation between below-cloud particle and in-cloud droplet composition for these four flights (in Figure 3) suggests that the more polluted flights had more chemical variability associated with pollution plumes and the daytime flights had more changes in supersaturation and mixing associated with diurnal heating.

[28] Figure 7 shows the droplet residual mass for each component plotted against the total mass of that component in-cloud (particle plus droplet) or below-cloud (particle only). Aliphatic C-C-H functional groups and sulfate ions dominate the composition, while mineral components constitute most of the remaining mass. Trace metals (vanadium, nickel, manganese, chromium, titanium, cobald, iron, and copper) have the lowest mass concentrations, typically with 1 to 10 ng m^{-3}. Table 6 summarizes the mass scavenging coefficients (F_{in} and F_{below}) and correlation coefficients for all six flights. The mean mass scavenging coefficients for the night flights in the DYCOMS-II study lie between 0.26 and 0.40 for interstitial particle concentrations (F_{in}, in-cloud mass scavenging coefficients) and between 0.14 and 0.68 for below-cloud particle concentrations (F_{below}, below-cloud mass scavenging coefficients), with each averaged over 18 chemical components. Droplet composition and particle composition within each flight and sample type (below-cloud versus in-cloud) are well correlated with slope uncertainties within ±0.06 in night flights and within ±0.11 in day flights. There is considerably more variation between the flights with factors of 1.5 and 4 separating the lowest and highest in-cloud and below-cloud average mass scavenging coefficients. One reason for this may be the variation in cloud supersaturation for different flights, which is inferred from the standard deviation of updraft velocity since supersaturation cannot be measured (Table 2). Flights 4 and 7 have consistent updraft velocities with standard deviations of 0.60–0.69 m s^{-1}. Flights 3 and 5 have more variability with ranges of 0.58–0.74 m s^{-1} and 0.43–0.66 m s^{-1}, respectively.

[29] Table 7 lists the day and night mass scavenging coefficients averaged over multiple flights for each component measured. Single-component F values are mostly between 0.2 and 0.4, with the least variation for nighttime in-cloud samples. Scavenging coefficients of the two most abundant components (aliphatic C-C-H and sulfate) have averages of 0.23 and 0.39, respectively. The correlation coefficients between the concentration of each compound in the particle phase and the concentration measured in the residual droplets is greater than 0.83 for 15 of the 16 comparisons and greater than or equal to 0.90 for 11 of the 16 comparisons (Table 6). This correlation is consistent with though not sufficient for internal mixing of the particles in the 0.2 to 1.3 μm diameter size range. The hygroscopic components had mass scavenging coefficients that were similar to less hygroscopic components, and hygroscopicity and mass scavenging were not correlated. For example, sulfate scavenging coefficients vary from 0.30 (below average efficiency) to 0.47 (above average efficiency) which is similar to sulfate mass scavenging reported by *Mertes et al.* [2001] where particles were mixtures of sulfate, organic carbon, sodium, and ammonium. The range of coefficients for sulfate suggests that the sulfate, organics, and other inorganic compounds may not have always been present in the same proportions or that variability in meteorological conditions and inlet efficiencies (see section 4.3) has influenced measured mass scavenging efficiencies. These findings are consistent with the conclusions of *Murphy et al.* [2006], who performed single-particle analysis using laser mass spectrometry and determined that over 90% of accumulation mode particles (0.1 to 1 μm) away from local sources were internal mixtures of sulfate and organics. The consistency in F over the 18 components strongly suggests that sea salt, sulfate, organics, trace metals, and mineral components are present as mixtures within the same particle types in submicron particles but is not sufficient to show that all particles are internally mixed, especially since activation and in-cloud scavenging processes are indistinguishable. However, the similarity of mass scavenging coefficients for multiple chemical components in the observed clouds means that the differences among the particle compositions do not have significant effects on their partitioning into droplets when cloud formation and processing mechanisms are considered together.

4.2. Submicron Below-Cloud Particle Mixtures With Sea Salt

[30] Single particle below-cloud TEM and SEM data for individual samples from flights 3, 5, and 7 are shown in Figure 8. Particles in the two smallest size channels are measured by TEM; those above 0.26 μm are measured by SEM. The particles are classified by K-means cluster analysis as employed by *Anderson et al.* [1996], resulting in simpler categories for the cleaner marine conditions of DYCOMS-II than the Bermuda particles: organic and soot

Table 6. Flight-Specific Mass Scavenging Coefficients With Correlation Coefficients Averaged Over All Chemical Components

	Below-Cloud		In-Cloud	
Flight	F_{below}[a]	R^2	F_{in}[a]	R^2
3	0.14 ± 0.02	0.83	0.40 ± 0.03	0.94
4	0.68 ± 0.06	0.92	0.28 ± 0.01	0.98
5	0.14 ± 0.01	0.94	0.27 ± 0.06	0.53
7	0.25 ± 0.01	0.98	0.26 ± 0.02	0.96
8	0.63 ± 0.04	0.90	0.29 ± 0.02	0.86
9	0.97 ± 0.11	0.90	0.47 ± 0.01	0.98
Night (3, 4, 5, 7)	0.17 ± 0.02	0.86	0.31 ± 0.03	0.86
Day (8, 9)	0.71 ± 0.06	0.90	0.37 ± 0.01	0.98

[a]Slopes and one standard deviations are calculated by a best-fit linear regression.

Table 7. Mean Mass Scavenging Coefficients for Each Measured Chemical Component[a]

	Below-Cloud		In-Cloud	
Species	Day Flights (8, 9)	Night Flights (3, 4, 5, 7)	Day Flights (8, 9)	Night Flights (3, 4, 5, 7)
Al	n/v[b]	n/v	0.27	0.4 ± 0.2[c]
Ca	0.30 ± 0.03	0.3 ± 0.1	0.3 ± 0.2	0.3 ± 0.1
C-C-H	0.31	0.3 ± 0.2	0.2 ± 0.1	0.2 ± 0.1
Cl	n/v	0.47 ± 0.09	0.5 ± 0.1	0.24 ± 0.06
Co	n/v	n/v	n/v	0.28
Cr	n/v	0.4 ± 0.2	0.41	0.3 ± 0.2
Cu	0.12	0.34 ± 0.05	0.38	0.27 ± 0.05
Fe	0.34 ± 0.02	0.4 ± 0.2	0.33 ± 0.08	0.3 ± 0.1
K	0.3 ± 0.2	0.2 ± 0.1	0.3 ± 0.1	0.2 ± 0.1
Mn	n/v	n/v	n/v	0.3 ± 0.2
NH_4	0.4 ± 0.2	0.27 ± 0.09	0.6 ± 0.6	0.23 ± 0.09
Ni	n/v	n/v	n/v	0.2 ± 0.1
S	0.26 ± 0.01	0.26	0.48 ± 0.05	0.5 ± 0.1
Si	0.3 ± 0.2	0.25 ± 0.07	0.23 ± 0.03	0.13 ± 0.06
SiO_4	0.54	0.17 ± 0.05	n/v	0.3 ± 0.1
SO_4	0.47 ± 0.09	0.3 ± 0.1	0.4 ± 0.2	0.4 ± 0.1
Ti	n/v	0.16 ± 0.06	n/v	0.38
V	0.3 ± 0.2	0.16	0.7 ± 0.4	0.26 ± 0.08

[a]Carbonyl C = O and organosulfur C-O-S were not present above detection limit in enough CVI samples to report individual mass scavenging values.
[b]n/v indicates no value, due to one or more components being below detection limits in the particle or droplet phase.
[c]The variability shown is the standard deviation of each component with more than one measurement above detection per flight.

(which are unresolved by SEM), unreacted sea salt (similar to categories 31–35, and 36 by *Anderson et al.* [1996]), reacted sea salt (categories 22–24, 30, 41, 43, 46, and 49), metal or mineral components (categories 1–21, 28, 38, 42, 44, 51, and 57), and ammonium sulfate (category 25), though no particles above 0.26 μm were classified as ammonium sulfate. Other sulfate salts (categories 26, 27, and 29) include calcium, magnesium, sodium and potassium sulfate and contain smaller amounts of sodium, and potassium than is expected for sea salt. These particles appear to be a mixed-cation sulfate that is part of normal sea salt but may have been mechanically separated from sodium chloride. Similar particles were observed by *Pósfai et al.* [1995] and *Anderson et al.* [1996]. Organic compounds that were internally mixed with sulfate or sea salt were not resolved by the weak carbon X-ray signal and may be underestimated or omitted. The bulk samples collected with the SDI for flights 3, 5, and 7 (Figures 3a and 3b) are similar in composition to the sea salt single particles described in Figure 8. The measured submicron composition from FTIR spectroscopy and XRF is consistent with the TEM and SEM results. The size-resolved composition from the TEM and SEM illustrate that for flights 3, 5, and 7, between 71% and 91% of particles with diameters larger than 0.26 μm had similar sea salt-containing compositions (internal mixtures of sea salt with varying ratios). Particles below 0.26 μm diameter have different and more variable compositions from the larger particles. Although these particles contribute a significant fraction to particle number the mass of these particles is too small to affect the mass-based scavenging coefficients for most chemical components.

4.3. Drop Size Effects on Inlet Efficiency and Mass Scavenging

[31] DYCOMS-II marine stratocumulus clouds are characterized by increasing droplet size with altitude (inferred from increasing liquid water content without changes in droplet number concentration [*Straub et al.*, 2007]), making the efficiency of the CVI for sampling drops increase with sampling altitude within clouds that contain some drops that are below this cutoff. Figure 9 shows that the fraction of droplets above 9 μm is correlated to normalized altitude $\overline{h}$

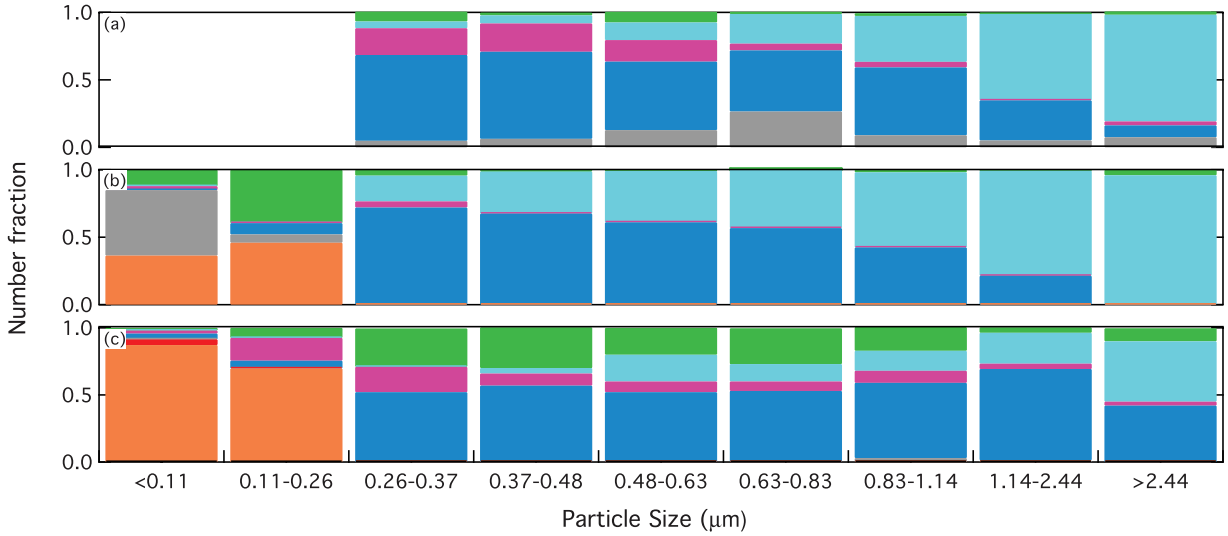

Figure 8. Size-resolved particle composition for the PCASP size range for flights (a) 3, (b) 5, and (c) 7. Transmission Electron Microscopy is used for $D_p < 0.26$ μm and Scanning Electron Microscopy for $D_p > 0.26$ μm. TEM measurements were not available for flight 3. Composition categories include: metals and mineral components (grey), ammonium sulfate (orange), unreacted sea salt (turquoise), partially and completely reacted sea salt (dark blue), other sulfate salts (magenta), and organics and soot (green). TEM size channels also include mixed (red) and unresolved (black) composition categories.

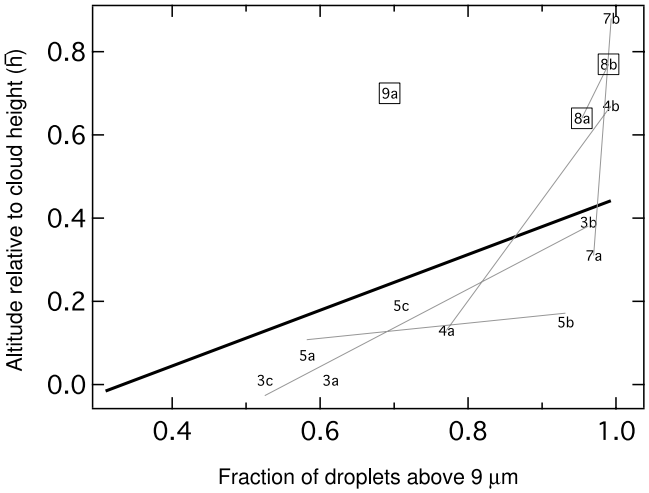

Figure 9. Fraction of droplets above 9 μm diameter as a function of $\overline{h}$, where $\overline{h}$ is the altitude of the sample within the cloud normalized by the cloud height (equation (7)). Each flight has either two or three droplet sampling intervals. The bold line represents the best fit ($y = 0.67\,h - 0.2$) of night flights (3, 4, 5, and 7); daytime flights 8 and 9 (boxed) were not included in the fit. Grey lines show the trend for individual flights and are a guide for the eye since there are 3 or fewer points in each fit.

for each sampling interval within the cloud (with $R^2 = 0.6$), with $\overline{h}$ calculated as

$$\overline{h} = \frac{z - z_{\text{base}}}{z_{\text{top}} - z_{\text{base}}} \tag{7}$$

(where z is the sample altitude and z_{base} and z_{top} are the cloud base and top altitudes, respectively). The samples taken closer to the cloud top contain a larger fraction of droplets above the lower CVI cutoff diameter as they coincide with the maximum liquid water content in the vertical profile (Figure 2).

[32] The calculation of mass scavenging coefficients is sensitive to the fraction of particles activated to droplets below 9 μm. The cutoff size D_p^* (equations (5) and (6)) is a function of the size distribution of the particles sampled, their composition (specifically the amount of soluble material in the particles), and the supersaturation. A measure of the representativeness of the mass scavenging coefficients of the entire droplet population is provided by the ratio of below-cloud D_p^* to $\overline{D}_{m,SDI}$. For ratios less than 1, the mean size is larger than the cutoff size, suggesting that more than 50% of below-cloud particles would activate to droplets greater than 9 μm. From the 11 below-cloud samples analyzed, 5 samples have ratios less than 1, indicating that the measured compositions of cloud droplet residuals are representative of at least 50% of the droplet population (Table 8).

[33] The mean mass PCASP diameter $\overline{D}_{m,PCASP}$ varies between 2.5 and 2.6 μm (Table 4). This diameter is approximately 1.5 times larger than the diameter of the particles collected through the SDI, which have $\overline{D}_m$ between 0.89 and 1.1 μm. The flights with the larger $\overline{D}_{m,SDI}$ (4, 7, and 8) are also the flights with the larger $\overline{D}_{m,PCASP}$. The SDI particle mass makes up between 3 to 4% of the 0.1 and 3.0 μm mass. Flight 7 is the cleanest flight, containing the lowest SDI number fraction and second lowest SDI mass fraction (Table 4).

[34] *Twohy et al.* [2005a] found that between 70% and 100% of particles (by number) in the nighttime below-cloud samples (in the PCASP size range of 0.1 to 3.0 μm) were scavenged to form droplets measured by the FSSP-100 and fast-FSSP in DYCOMS-II [Figure 3, *Twohy et al.*, 2005a], while the nighttime mass scavenging coefficients reported here are between 14% and 68% below-cloud (Table 6). This difference is attributed to the missed activated mass in droplets between 2 μm (lower FSSP-100 limit) and 9 μm (lower CVI limit), which yields mass scavenging coefficients that are biased low relative to a hypothetical inlet that collects all cloud drops. This difference is larger for flights with small average drop diameters (flights 3, 5, and 9) and for samples collected near cloud bottom. The dependence of mass scavenging coefficient on drop size in Figure 10 shows a consistent increase in mass scavenging coefficient of night flights with an increasing fraction of drops above 9 μm. Three flights (4, 8, and 9) contained samples with more than 50% of the particle mass collected by the CVI were within the flight to flight variability of the number activation reported by *Twohy et al.* [2005a].

5. Conclusion

[35] The 0.2 to 1.3 μm particles sampled in and below-cloud during DYCOMS-II partition to cloud droplets as if they are internally mixed, consistent with the SEM composition measurements showing that most particles between 0.26 μm and 1.14 μm are internal mixtures with reacted and unreacted sea salt. The 18 measured organic and inorganic functional groups, mineral components, and trace metals show nighttime in-cloud mass scavenging coefficients between 26% and 47% for droplets larger than 9 μm diameter. For each flight and sample type (in-cloud or below-cloud) there is little variation between component-specific mass scavenging coefficients, even for components with different

Table 8. Inferred Cutoff Diameter D_p^* for Collection of Droplets in the CVI[a]

Flight	Below-Cloud, μm	In-Cloud, μm	Ratio of Below-Cloud D^*_p to $\overline{D}_{m,SDI}$[b]
3	1.0	1.1	2.1
	1.2	1.1	1.7
		1.1	
4	0.26	1.2	0.50
	0.26	1.2	0.49
5	1.1	1.1	1.8
	1.1	1.2	1.7
		1.2	
7	0.98	1.2	1.6
	1.1	1.2	1.7
8	0.26	1.2	0.51
	0.26	1.2	0.49
9	0.22	1.1	0.33
		0.22	

[a]Values were interpolated between bin edges to give a best estimate. Bin sizes were 0.1 μm for flights 3, 5, and 7 and 0.02 μm for flights 4, 8, and 9. Multiple samples were obtained during each flight.

[b]$\overline{D}_{m,SDI}$ is the mass-mean diameter of particles between 0.2 and 1.3 μm.

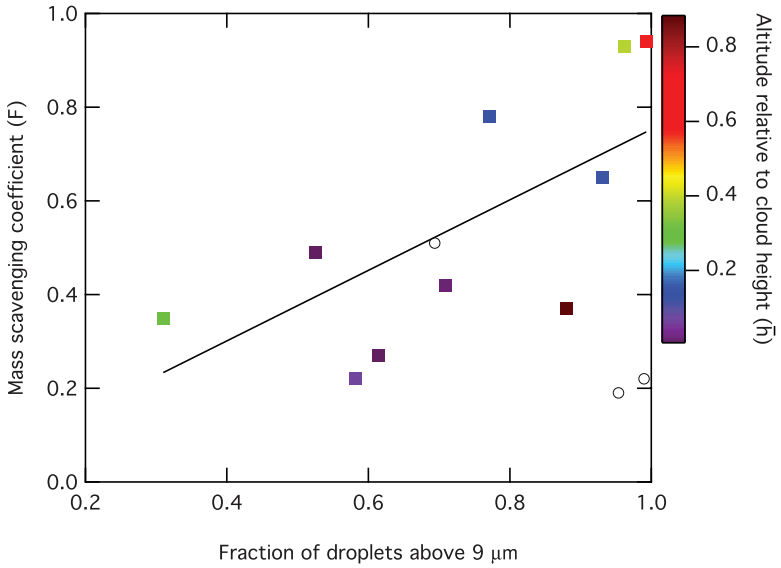

Figure 10. Mass scavenging fraction as a function of the fraction of droplets above 9 μm for each interstitial sample. Each flight has multiple samples. The best fit through nighttime flights 3, 4, 5, and 7 (square markers) is y = 0.75x (black line); daytime flights 8 and 9 are symbolized with open circles. Color indicates the sample altitude normalized relative to cloud height $\overline{h}$, as given in equation (7).

hygroscopicity. Flight 4 has clean marine conditions, well-mixed and consistent ozone mixing ratios, and very similar variations in updraft velocity throughout the flight resulting in a droplet residual composition that is very similar to the below-cloud particle composition. SEM measurements for flights 3, 5, and 7 show that greater than 90% of the number of particles above 0.26 μm are internal mixtures of sea salt, sulfate and nitrate, with XRF and FTIR measurements identifying organic compounds and trace metals in this 0.8 μm mode. For 5 of the 11 CVI samples, more than half of the below-cloud particles were larger than the CVI cutoff size for particles activating to droplets larger than 9 μm. Droplets missed below 9 μm diameter biased the scavenging coefficients low (especially for lower cloud altitudes and smaller drop sizes) but do not affect the observed uniformity of mass scavenging coefficients for the 18 components measured.

[36] For the particle compositions sampled during DYCOMS-II, substantial physical and chemical evidence show that the measured chemical components partition between particle and droplet phases as if they are internally mixed. The combination of SEM identification of sea salt in 90% of the 0.8 μm-mode particles with physical measurements of uniform particle-droplet partitioning means that the scavenged fraction of particles behave as if the components were internally mixed in the particles.

[37] Extrapolating these results to other meteorological conditions, sources, and locations is not warranted, as the particles sampled here are unique in their distance from sources (300 km offshore) with substantial time for prior processing in cloud layers. The low supersaturations of Pacific marine stratocumulus also mean larger activation diameters such that the smaller, less processed particles (which are externally mixed in many of the components measured here) do not contribute substantially to activated droplet mass. Studies of particle and droplet composition in other locations are needed to provide a more complete description of the partitioning of chemical components in other aerosol-cloud interactions.

[38] **Acknowledgments.** This work was supported by the National Science Foundation under grant ATM01-04707 and by the National Oceanic and Atmospheric Administration under grant NA17RJ1231. We thank Monica Rivera and Steve Maria for assistance in sample collection and analysis, and Jean-Louis Brenguier and Frederic Burnet for the flight 5 Fast-FSSP data. We also acknowledge NCAR RAF, including Krista Laursen and Chris Webster, for project and field assistance and Teresa Campos for ozone mixing ratio measurements.

References

Allan, J., et al. (2004), Submicron aerosol composition at Trinidad Head, California, during ITCT 2K2: Its relationship with gas phase volatile organic carbon and assessment of instrument performance, *J. Geophys. Res.*, *109*, D23S24, doi:10.1029/2003JD004208.

Anderson, J. R., P. R. Buseck, T. L. Patterson, and R. Arimoto (1996), Characterization of the Bermuda tropospheric aerosol by combined individual-particle and bulk-aerosol analysis, *Atmos. Environ.*, *30*(2), 319–338.

Baltensperger, U., M. Schwikowski, D. T. Jost, S. Nyeki, H. W. Gaggeler, and O. Poulida (1998), Scavenging of atmospheric constituents in mixed phase clouds at the high alpine site Jungfraujoch, Part I: Basic concept and aerosol scavenging clouds, *Atmos. Environ.*, *32*(23), 3975–3983.

Boskovic, L., I. S. Altman, I. E. Agranovski, R. D. Braddock, T. Myojo, and M. Choi (2005), Influence of particle shape on filtration processes, *Aeros. Sci. Tech.*, *39*(12), 1184–1190, doi:10.1080/02786820500442410.

Brach, R. M., P. F. Dunn, and X. Li (2000), Experiments and engineering models of microparticle impact and deposition, *J. Adhesion*, *74*(1), 227–282, doi:10.1080/00218460008034531.

Brenguier, J. L., T. Bourrianne, A. D. Coelho, J. Isbert, R. Peytavi, D. Trevarin, and P. Weschler (1998), Improvements of droplet size distribution measurements with the Fast-FSSP (Forward Scattering Spectrometer Probe), *J. Atmos. Ocean Technol.*, *15*(5), 1077–1090.

Brock, C. A., et al. (2004), Particle characteristics following cloud-modified transport from Asia to North America, *J. Geophys. Res.*, *109*, D23S26, doi:10.1029/2003JD004198.

Burnet, F., and J. L. Brenguier (2002), Comparison between Standard and Modified Forward Scattering Spectrometer Probes during the Small Cumulus Microphysics Study, *J. Atmos. Ocean Technol.*, *19*, 1516–1531.

Charlson, R. J., S. E. Schwartz, J. M. Hales, R. D. Cess, J. A. Coakley Jr., J. E. Hansen, and D. J. Hoffman (1992), Climate forcing by anthropogenic aerosols, *Science*, *255*, 423–430.

Corrigan, C. E., and T. Novakov (1999), Cloud condensation nucleus activity of organic compounds: A laboratory study, *Atmos. Environ.*, *33*, 2661–2668.

Cziczo, D. J., D. M. Murphy, P. K. Hudson, and D. S. Thomson (2004), Single particle measurements of the chemical composition of cirrus ice residue during CRYSTAL-FACE, *J. Geophys. Res.*, *109*, D04201, doi:10.1029/2003JD004032.

Dusek, U., et al. (2006), Size matters more than chemistry for cloud-nucleating ability of aerosol particles, *Science*, *312*(5778), 1375–1378.

Ervens, B., M. Cubison, E. Andrews, G. Feingold, J. A. Ogren, J. L. Jimenez, P. DeCarlo, and A. Nenes (2007), Prediction of cloud condensation nucleus number concentration using measurements of aerosol size distributions and composition and light scattering enhancement due to humidity, *J. Geophys. Res.*, *112*, D10S32, doi:10.1029/2006JD007426.

Facchini, M. C., et al. (1999), Partitioning of the organic aerosol component between fog droplets and interstitial air, *J. Geophys. Res.*, *104*(D21), 26,821–26,832.

Gao, Y., and J. R. Anderson (2001), Characteristics of Chinese aerosols determined by individual-particle analysis, *J. Geophys. Res.*, *106*(D16), 18,037–18,045.

Hallberg, A., J. A. Ogren, K. J. Noone, J. Heintzenberg, A. Berner, I. Solly, C. Kruisz, G. Reische, S. Fuzzi, and M. C. Facchini (1992), Phase partitioning for different aerosol species in fog, *Chem. Phys. Meteorol.*, *44B*(5), 545–555.

Hansson, H.-C., M. J. Rood, S. Koloutsou-Vakakis, K. Hämeri, D. Orsini, and A. Wiedensohler (1998), NaCl aerosol particle hygroscopicity dependence on mixing with organic compounds, *J. Atmos. Chem.*, *31*, 321–346.

Hegg, D. A., R. J. Ferek, and P. V. Hobbs (1993), Aerosol size distributions in the cloudy atmospheric boundary-layer of the North Atlantic Ocean, *J. Geophys. Res.*, *98*(D5), 8841–8846.

Heintzenberg, J., and C. Leck (1994), Seasonal variation of the atmospheric aerosol near the top of the marine boundary layer over Spitsbergen related to the Arctic sulphur cycle, *Tellus*, *46B*, 52–67.

Huebert, B. J., et al. (2004), PELTI: Measuring the passing efficiency of an airborne low turbulence aerosol inlet, *Aerosol Sci. Technol.*, *38*, 803–826, doi:10.1080/027868290500823.

Kondo, Y., Y. Miyazaki, N. Takegawa, T. Miyakawa, R. J. Weber, J. L. Jimenez, Q. Zhang, and D. R. Worsnop (2007), Oxygenated and water-soluble organic aerosols in Tokyo, *J. Geophys. Res.*, *112*, D01203, doi:10.1029/2006JD007056.

Lee, S.-H., D. M. Murphy, D. S. Thomson, and A. M. Middlebrook (2002), Chemical components of single particles measured with Particle Analysis by Laser Mass Spectrometry (PALMS) during the Atlanta SuperSite Project: Focus on organic/sulfate, lead, soot, and mineral particles, *J. Geophys. Res.*, *107*(D1), 4003, doi:10.1029/2000JD000011.

Levin, Z., A. Teller, E. Ganor, B. Graham, M. O. Andreae, W. Maenhaut, A. H. Falkovich, and Y. Rudich (2003), Role of aerosol size and composition in nucleation scavenging within clouds in a shallow cold front, *J. Geophys. Res.*, *108*(D22), 4700, doi:10.1029/2003JD003647.

Li, J., J. R. Anderson, and P. R. Buseck (2003), TEM study of aerosol particles from clean and polluted marine boundary layers over the North Atlantic, *J. Geophys. Res.*, *108*(D6), 4189, doi:10.1029/2002JD002106.

Maria, S. F., and L. M. Russell (2005), Organic and inorganic aerosol below-cloud scavenging by suburban New Jersey precipitation, *Environ. Sci. Technol.*, *39*(13), 4793–4800.

Maria, S. F., L. M. Russell, B. J. Turpin, and R. J. Porcja (2002), FTIR measurements of functional groups and organic mass in aerosol samples over the Caribbean, *Atmos. Environ.*, *36*, 5185–5196.

Maria, S. F., L. M. Russell, B. J. Turpin, R. J. Porcja, T. L. Campos, R. J. Weber, and B. J. Huebert (2003), Source signatures of carbon monoxide and organic functional groups in Asian Pacific Regional Aerosol Characterization Experiment (ACE-Asia) submicron aerosol types, *J. Geophys. Res.*, *108*(D23), 8637, doi:10.1029/2003JD003703.

Mertes, S., A. Schwarzenbock, E. Bruggeman, T. Gnauk, and B. Dippel (2001), Phase partitioning of black carbon, non-volatile organic carbon and soluble inorganic substances between the droplet and interstitial phase of clouds at Mt. Brocken, Germany, *J. Aerosol Sci.*, *32*(1001), 969–980.

Middlebrook, A. M., D. M. Murphy, and D. S. Thomson (1998), Observations of organic material in individual marine particles at Cape Grim during the First Aerosol Characterization Experiment (ACE 1), *J. Geophys. Res.*, *103*(D13), 16,475–16,483.

Ming, Y., and L. M. Russell (2004), Organic aerosol effects on fog droplet spectra, *J. Geophys. Res.*, *109*, D10206, doi:10.1029/2003JD004427.

Murphy, D. M., and D. S. Thomson (1997), Chemical composition of single aerosol particles at Idaho Hill: Negative ion measurements, *J. Geophys. Res.*, *102*(D5), 6353–6368.

Murphy, D. M., D. S. Thomson, and M. J. Mahoney (1998), In situ measurements of organics, meteoric material, mercury, and other elements in aerosols at 5 to 19 kilometers, *Science*, *282*, 1664–1669.

Murphy, D. M., D. J. Cziczo, K. D. Froyd, P. K. Hudson, B. M. Matthew, A. M. Middlebrook, R. E. Peltier, A. Sullivan, D. S. Thomson, and R. L. Weber (2006), Single-particle mass spectrometry of tropospheric aerosol particles, *J. Geophys. Res.*, *111*(D23), D23S32, doi:10.1029/2006JD007340.

O'Dowd, C. D., J. A. Lowe, and M. H. Smith (1999), Observations and modelling of aerosol growth in marine stratocumulus - Case study, *Atmos. Environ.*, *33*, 3053–3062.

Pósfai, M., J. R. Anderson, P. R. Buseck, and H. Sievering (1995), Compositional variations of sea-salt-mode aerosol particles from the North Atlantic, *J. Geophys. Res.*, *100*(D11), 23,063–23,074.

Seinfeld, J. H., and S. N. Pandis (1998), *Atmospheric Chemistry and Physics*, John Wiley , New York.

Sellegri, K., P. Laj, R. Dupuy, M. Legrand, S. Preunkert, and J. P. Putaud (2003), Size-dependent scavenging efficiencies of multicomponent atmospheric aerosols in clouds, *J. Geophys. Res.*, *108*(D11), 4334, doi:10.1029/2002JD002749.

Stevens, B., et al. (2003), Dynamics and Chemistry of Marine Stratocumulus-DYCOMS-II, *Bull. Am. Meteorol. Soc.*, *84*, 51–57.

Strapp, J., W. R. Leaitch, and P. S. K. Liu (1992), Hydrated and dried aerosol-size-distribution measurements from the Particle Measuring Systems FSSP-300 probe and deiced PCASP-100x probe, *J. Atmos. Oceanic Technol.*, *9*, 548–555.

Straub, D., T. Lee, and J. L. Collett Jr. (2007), The chemical composition of marine stratocumulus clouds over the eastern Pacific Ocean, *J. Geophys. Res.*, *112*(D4), D04307, doi:10.1029/2006JD007439.

Sugimoto, N., I. Matsui, A. Shimizu, I. Uno, K. Asai, T. Endoh, and T. Nakajima (2002), Observation of dust and anthropogenic aerosol plumes in the Northwest Pacific with a two-wavelength polarization lidar on board the research vessel Mirai, *Geophys. Res. Lett.*, *29*(19), 1901, doi:10.1029/2002GL015112.

Twohy, C. H., J. G. Hudson, S.-S. Yum, J. R. Anderson, S. K. Durlak, and D. Baumgardner (2001), Characterisitics of cloud-nucleating aerosols in the Indian Ocean, *J. Geophys. Res.*, *106*(D22), 28,699–28,710.

Twohy, C. H., M. D. Petters, J. R. Snider, B. Stevens, W. Tahnk, M. Wetzel, L. M. Russell, and F. Burnet (2005a), Evaluation of the aerosol indirect effect in marine stratocumulus clouds: Droplet number, size, liquid water path, and radiative impact, *J. Geophys. Res.*, *110*, D08203, doi:10.1029/2004JD005116.

Twohy, C. H., J. R. Anderson, and P. A. Crozier (2005b), Nitrogenated organic aerosols as cloud condensation nuclei, *Geophys. Res. Lett.*, *32*, L19805, doi:10.1029/2005GL023605.

Twomey, S. (1977), The influence of pollution on the shortwave albedo of clouds, *J. Atmos. Sci.*, *34*, 1149–1152.

Väkevä, M., K. Hämeri, and P. P. Alto (2002), Hygroscopic properties of nucleation mode and Aitken mode particles during nucleation bursts in background air on the west coast of Ireland, *J. Geophys. Res.*, *107*(D19), 8104, doi:10.1029/2000JD000176.

vanZanten, M. C., B. Stevens, G. Vali, and D. H. Lenschow (2005), Observations of drizzle in marine stratocumulus, *J. Atmos. Sci.*, *62*(1), 88–106.

Warneck, P. (1988), *Chemistry of the Natural Atmosphere*, Elsevier, London.

J. R. Anderson, Environmental Fluid Dynamics Program, Department of Mechanical and Aerospace Engineering, Arizona State University, Mail Code 6106, P.O. Box 876106, Tempe, AZ 85287-6106, USA.

L. N. Hawkins and L. M. Russell, Scripps Institution of Oceanography, University of California San Diego, 9500 Gilman Dr., Mail Code 0221, La Jolla, CA 92093-0221, USA. (lmrussell@ucsd.edu)

C. H. Twohy, College of Oceanography and Atmospheric Sciences Oceanography, Admin 104, Oregon State University, Corvallis, OR 97331-5503, USA.